



# Effect of additive manufactured lattice defects on mechanical properties: an automated method for the enhancement of lattice geometry

Ahmad Alghamdi<sup>1,2</sup> · Tobias Maconachie<sup>1,3</sup> · David Downing<sup>1,4</sup> · Milan Brandt<sup>1,4</sup> · Ma Qian<sup>1</sup> · Martin Leary<sup>1,3,4</sup>

Received: 23 December 2019 / Accepted: 1 May 2020 / Published online: 25 May 2020  
© Springer-Verlag London Ltd., part of Springer Nature 2020

## Abstract

Metal additive manufacturing (MAM) enables the fabrication of structures with complexity and resolution that cannot be achieved by traditional manufacturing techniques, including lattice structures. However, MAM processes inherently induce local manufacturing defects, resulting in variation between the idealised and as-manufactured geometry and potentially introducing stress concentrations that are detrimental to structural performance. Quantification of these effects on mechanical performance enables the manipulation of intended lattice geometry to enhance structural performance. However, due to the geometric complexity and small scale of geometric defects, experimental testing and numerical simulation of lattice structures are technically difficult and time-consuming. To overcome this limitation, a novel methodology for quantifying the effect of manufacturing defects on the mechanical properties of MAM lattice structural elements is proposed. This method involves the automated analysis of microscope images of as-manufactured lattice structures to generate numerical models that automate the identification of plastic hinge behaviour in node elements based on custom MAM material properties. This method is applied to Ti-6Al-4V lattice structures fabricated by selective laser melting (SLM) with a range of strut and node diameters and cell sizes. This novel method is shown to predict the effect of local manufacturing defects on bulk lattice mechanical response and provides an efficient tool for the optimisation of as-manufactured MAM lattice structures.

**Keywords** Metal additive manufacturing · Lattice structures · Numerical modelling · Manufacturing defects · Design for additive manufacturing · Selective laser melting

## 1 Introduction

The commercial development of metallic additive manufacturing (MAM) techniques, particularly selective laser melting (SLM), has enabled the fabrication of sophisticated

components with high complexity and fine details that are not manufacturable with traditional methods. For example, lattice structures which are three-dimensional topologically ordered, open-celled structures composed of an arrangement of interacting unit cells [1]. The geometry and topology of these unit cells can be tuned to produce a range of useful properties [2], and as a result, MAM lattice structures have received much research attention, particularly for aerospace [3] and biomedical [4] applications.

However, MAM processes inherently induce geometric defects that significantly affect the performance of fabricated components. These as-manufactured defects may be inherent to the MAM process, for example stair-step geometry, or may be caused by sub-optimal process parameters [5] or the surface adhesion of partially melted particles [6]. Emerging research has demonstrated that geometric size effects are predictable for geometry of interest based on experimental

---

✉ Martin Leary  
martin.leary@rmit.edu.au

<sup>1</sup> RMIT Centre for Additive Manufacture, School of Engineering, RMIT University, Melbourne, Australia

<sup>2</sup> College of Engineering in Al-Qunfudhah, Umm Al-Qura University, Mecca, Kingdom of Saudi Arabia

<sup>3</sup> ARC Training Centre for Lightweight Automotive Structures (ATLAS), Melbourne, Australia

<sup>4</sup> ARC Training Centre in Additive Biomanufacturing, Brisbane, Australia

observation [7]. Furthermore, residual stresses resulting from the significant thermal gradients experienced by MAM components during manufacture may also cause geometric defects such as distortion of features or severe notches [8]. Specifically for mechanically loaded MAM lattice structures, geometric defects introduce stress concentrations reducing strength and stiffness [9].

Quantification of the effects of as-manufactured geometric defects on lattice structural response requires experimental testing or numerical simulation. These methods are technically challenging and time-consuming due to the large number of individual strut elements within a typical lattice structure, the large number of geometric parameters of interest, and the relatively small scale of specific geometric defects. To overcome this limitation, a methodology is proposed for the computationally efficient characterisation of the effect of geometric errors on the mechanical performance of MAM lattice structures.

Specifically, the methodology generates computationally efficient numerical models based on automated analysis of transmitted light microscope images of as-manufactured lattice specimens and experimentally derived bulk MAM material properties. Custom methods are developed to automate the identification of a plastic hinge through all strut elements in the unit cell. Outcomes of this analysis enable quantification of the effects of geometric defects on the mechanical properties of as-manufactured lattice specimens and can be used to improve the design and performance of lattice structures.

To demonstrate the capabilities of this method, Ti-6Al-4V lattice structures manufactured by SLM were acquired and analysed. These lattice structures were manufactured with a range of strut and node diameters, as well as cell sizes. Finite element (FE) models were then generated based on this geometric data to provide insight into the relationship between idealised CAD and as-manufactured geometry, as well as the effects of lattice element geometry and geometric defects on mechanical performance.

Boundary conditions and displacements are automatically applied based on the observed geometry of the numerical models, and reaction forces and internal stresses are automatically measured. These displacements are applied iteratively until the defined failure criterion is met, which in this case is defined as the displacement at which a plastic hinge occurs in all strut elements. A database of strength and stiffness of the analysed unit cells is then exported including design data for the idealised CAD geometry. The automated data flow of the proposed methodology enables the effective characterisation of the effect of as-manufactured lattice defects on mechanical response. Although this implementation is based on a failure criterion of a critical plastic hinge developing in the lattice unit cell, the methodology is fundamentally compatible with alternate failure criterion, including fatigue, energy absorption, thermal conductivity, and vibration.

This research explores the general properties and performance of lattice structures, followed by a review of the literature of geometric defects associated with MAM. A detailed description of the proposed method is provided, as well as insights into the effects of node size and manufacturing defects on the performance of the candidate lattice structures.

## 2 Lattice structures

The technical advantages of cellular structures have been understood for some time [10], including excellent strength to weight ratios and the potential for an extended plateau of the force-displacement curve as is required for energy absorption applications [11]. A range of cellular structures have been manufactured using a variety of methods, including metallic foams [12] and composite honeycomb sandwich structures [13]. However, modern MAM techniques have enabled the fabrication of sophisticated lattice structures with bespoke unit cell topology and associated local geometry [14].

The general behaviour of lattice structures can be predicted by the Maxwell criterion ( $M$ ) (Eqs. 1 and 2) based on the number of struts ( $s$ ) and nodes ( $n$ ) within the lattice unit cell for a given dimensionality [15]. If  $M < 0$ , there are too few struts to equilibrate bending moments at nodes, meaning that strut elements experience bending stresses; these structures are referred to as being *bending-dominated* (Fig. 1(a)) and are characterised by compliant force-displacement behaviour. If  $M \geq 0$ , sufficient strut elements exist to equilibrate externally applied forces, meaning that strut elements only experience axial stresses. These structures are referred to as *stretch-dominated* (Fig. 1(b)) and are stronger and stiffer than bending-dominated structures.

$$M = s - 2n + 3 \quad (\text{two-dimensional truss}) \quad (1)$$

$$M = s - 3n + 6 \quad (\text{three-dimensional truss}) \quad (2)$$

Lattice structure unit cell topologies are defined by the connectivity of their constituent node and strut elements (Fig. 1). The topology of the lattice unit cell considered in this work is referred to as face-centred cubic (FCC) (Fig. 2), after

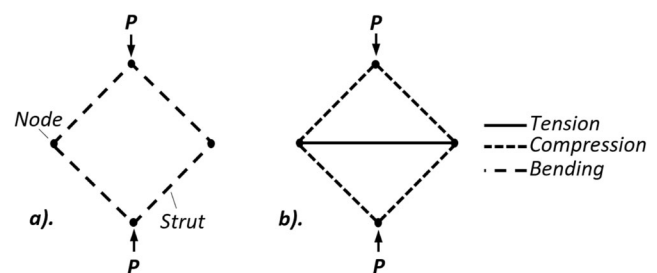


Fig. 1 Examples of (a) bending-dominated and (b) stretch-dominated lattice structures

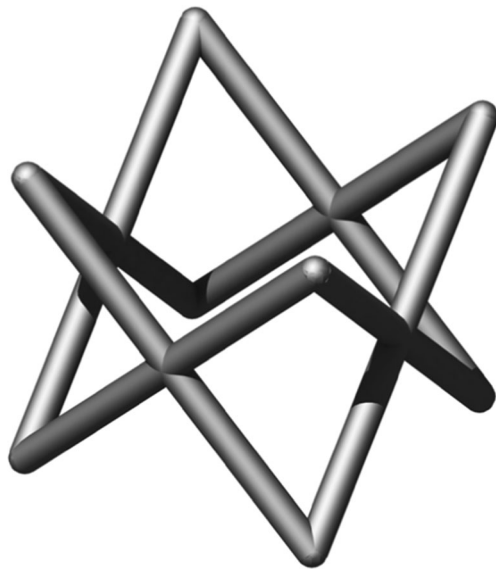


Fig. 2 Face-centred cubic (FCC) lattice structure unit cell

the analogous crystalline structure, consistent with previous studies [10, 15, 16]. FCC unit cells have twelve nodes and sixteen struts per unit cell. This means these unit cells have a Maxwell number of  $-14$  and so are considered bending-dominated.

### 3 Geometric defects of MAM lattice structures

Components fabricated by additive manufacturing (AM) processes are prone to inherent geometric defects. For example, the layer-wise method of additive manufacture causes the stair-stepping effect and may lead to layer defects [16]. There is also a minimum inclination angle<sup>1</sup> below which components cannot be confidently manufactured, which is dependent on a range of geometric and processing parameters, but is generally assumed to be approximately  $45^\circ$  [17].

There also exist geometric defects specific to particular MAM processes. Selective laser melting (SLM) and electron beam melting (EBM) are complex thermo-mechanical processes in which manufactured components experience extreme local thermal gradients [18]. This thermal behaviour affects the microstructure of fabricated components, can result in residual stresses within components, and may lead to geometric defects such as warping or severe notches [19]. These properties and defects (Fig. 3) lead to discrepancies between idealised CAD and as-manufactured geometry resulting in unanticipated mechanical response of as-manufactured MAM lattice structures (Fig. 4).

<sup>1</sup> Inclination angle is the angle between the build platen and a downward-facing surface.

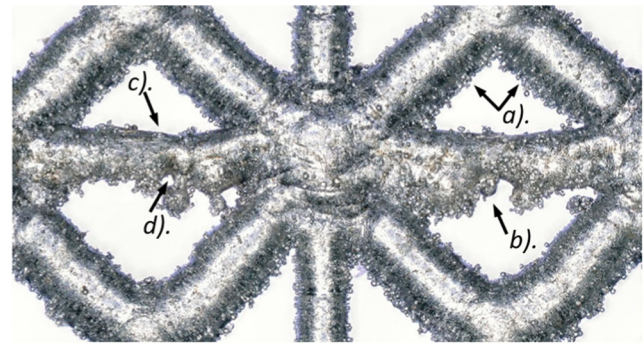


Fig. 3 As-manufactured lattice geometry including potential defects. (a) Adhered powder particles over the surface of the struts. (b) Large partially attached globule on surface. (c) Badly formed struts due to low inclination angle. (d) Severe notch in strut

### 3.1 Review of manufacturing defects associated with MAM

A review of localised manufacturing defects reported for MAM in the literature identifies the following relevant findings:

- Yavari et al. investigated the effects of lattice unit cell topology on the porosity and fatigue performance of Ti-6Al-4V lattice structures manufactured by SLM [20]. Investigation of cube, diamond, and truncated cuboctahedron unit cells found that structures with cube

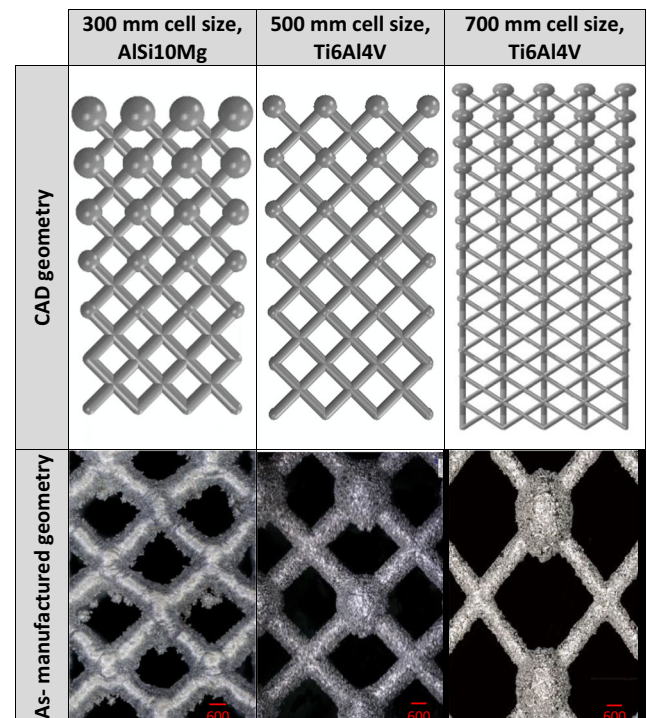
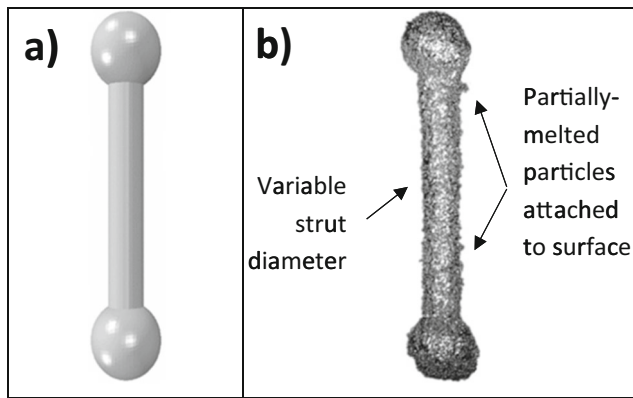
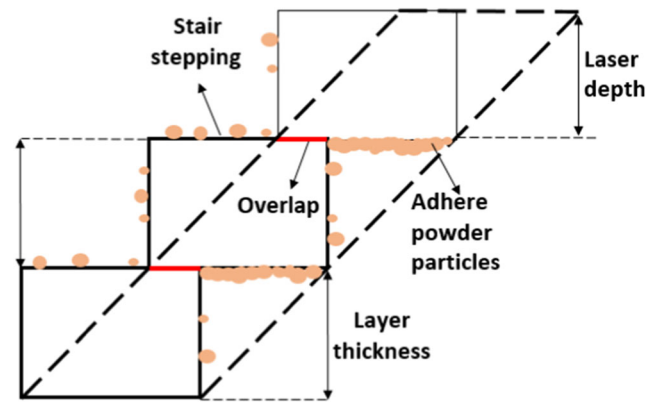


Fig. 4 Qualitative comparison of variation observed between idealised CAD and as-manufactured geometries for lattices with different cell sizes and materials of manufacture



**Fig. 5** a Idealised CAD and (b) As-manufactured geometry of lattice strut element manufactured in Ti-6Al-4V by SLM



**Fig. 7** Schematic representation of partially melted particles bound to the downward-facing surfaces in the SLM process [9]

unit cells have fewer notches and manufacturing imperfections than the other topologies, and relatively low variation in strut diameter; comparatively, structures with diamond unit cells were observed to have the greatest number of imperfections. These differences were reflected in the fatigue behaviour of these structures, with cube unit cell structures outperforming the other investigated topologies.

- Wauthle et al. investigated the effect of build orientation and various post-processing heat treatments on the mechanical performance and microstructure of Ti-6Al-4V lattice structures manufactured by SLM [19]. The orientation of strut elements was found to significantly affect structural performance, with horizontally oriented strut elements being highly defective, resulting in a significant reduction in strength. Heat treatment was identified as a means of increasing stiffness and ductility but not entirely overcoming losses to defects due to build orientation.
- Santorinaios et al., who studied the compressive behaviour of stainless steel lattice structures fabricated with

SLM, found that horizontal struts could not be manufactured [21]. Geometric imperfections were observed in as-manufactured struts, demonstrating the importance of optimised processing parameters to mitigate the effect of these defects.

- Yan et al. evaluated the effects of manufacturability and compressive performance of stainless steel lattice structures with gyroid unit cells manufactured by SLM. Good agreement was observed between idealised and as-manufactured geometries [22]. A large range of unit cell sizes was found to be manufacturable, although post-manufacture powder removal was difficult for very small cell sizes. Unit cells larger than 5 mm could not be manufactured as they were more prone to deformation during manufacture due to longer struts increasing the length of overhangs.
- Leary et al. investigated the mechanical properties and manufacturability of AlSi12Mg lattice structures manufactured by SLM [15]. Limitations of the SLM process were found to constrain the viability of lattice strut orientations, as struts with low inclination angles require support structures and are consequently infeasible for lattice structures. Struts with diameters ranging from 0.5 to 3.0 mm were found to be manufacturable if the angle

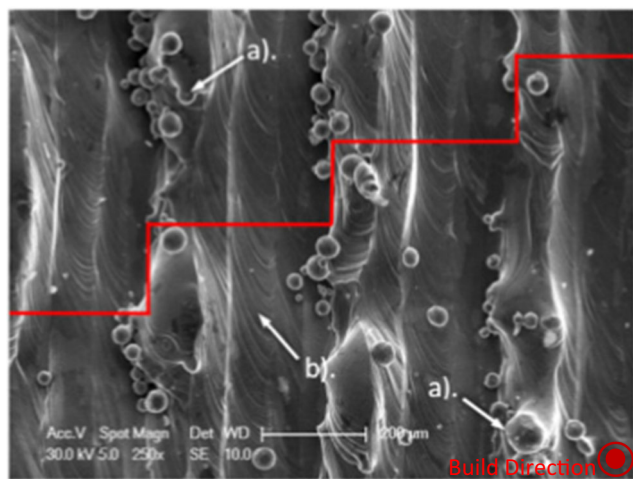


**Fig. 6** SEM micrograph of upward-facing surface of SLM-manufactured Ti-6Al-4V. Line indicates stair-step profile due to discrete addition of sequential layers. a Partially adhered powder particles and (b) teardrop profiles of fused laser melt pool are visible

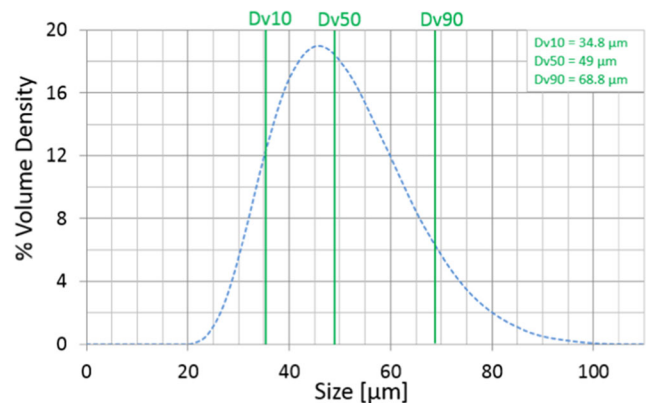


**Fig. 8** Particle size distribution of Ti-6Al-4V powder used for lattice manufacture

between the strut and the build platen was greater than 35°. The downward-facing surfaces of struts were consistently found to have significantly greater surface roughness, and many geometric defects were identified at the node elements.

### 3.2 Examples of as-manufactured MAM lattice structure defects

An individual lattice structure strut is presented to demonstrate the geometric complexity of the potential imperfections of as-manufactured elements, such as a variable diameter, malformed node elements, and semi-melted powder particles attached to the surface (Fig. 5).

### 3.3 Surface roughness of MAM components

The surface quality of as-manufactured MAM components remains a technical challenge for commercial applications, potentially necessitating post-processing, thereby increasing unit cost and lead times [23]. Surface quality has been found to be particularly important for the fatigue-life of dynamically loaded components as surface defects may cause early crack initiation and growth [20].

Surface roughness of MAM may be caused by the stair-step phenomena inherent to layer-wise MAM systems [24]. For example, the scanning electron microscope (SEM) micrograph presented in Fig. 6 identifies high surface roughness with the stair-step effect being clearly visible, especially surfaces with low inclination angles.

The attachment of partially melted particles to downward-facing surfaces during powder bed MAM manufacture is another cause of surface roughness. This phenomenon is schematically illustrated in Fig. 7, whereby the supporting powder bed is exposed to significant thermal loading resulting in partially melted powder particles being bound to the newly formed layer by thermal diffusion through the powder bed [9, 25]. Experimental results indicate that these particles are of spherical shape and are therefore caused by partial melting, and that smaller particle sizes may therefore be beneficial to reduce overall surface roughness [9].

The surface roughness of MAM specimens may also be affected by the ‘balling’ phenomenon whereby sub-optimal

process parameters result in discretisation of the melt pool track [26]. Balling can contribute to internal porosity [27] and is detrimental to the surface quality of MAM components [22].

However, surface roughness may also be an advantage, particularly for biomedical applications where studies have identified a link between surface roughness and cell attachment [28–30] and bone integration [31–34].

### 3.4 Residual stresses resulting from the MAM process

During the SLM process, manufactured structures are rapidly heated and cooled, inducing residual stresses within the solid structure that may cause cracking or deformation [35].

Liu et al. [36] investigated the position and magnitude of residual stresses within SLM components. They found stresses parallel to the laser scanning path to be more significant than stresses perpendicular to the scanning path, and that residual stresses peak at the onset of scanning paths.

Heating of the powder bed can reduce the temperature differential during manufacture, leading to reduced residual stress effects. For example, Ali et al. [37] were able to improve the yield strength and ductility of Ti-6Al-4V specimens fabricated by SLM by preheating the powder bed and reduce residual stresses. Furthermore, post-fabrication heat treatment can be applied to mitigate residual stress effects.

The effects of residual stresses are not currently accommodated within the proposed methodology; however, this capability can be extended by future researchers if appropriate experimental methods to acquire residual stress fields can be developed.

## 4 Method and material

In this research, a methodology for characterising effect of geometric irregularities on the mechanical properties of MAM lattice structures is proposed. A 2D FE model is generated based on transmitted light images of as-manufactured lattice structures combined with experimentally derived material properties. Displacement is iteratively applied to the model until the specified failure criterion is met, which is here defined as the displacement at which plastic hinges form in each of the analysed struts. Reaction forces and internal stress are measured to quantify the strength, stiffness, and associated stresses present within the model. Details of the methodology are presented below for a MAM application of interest.

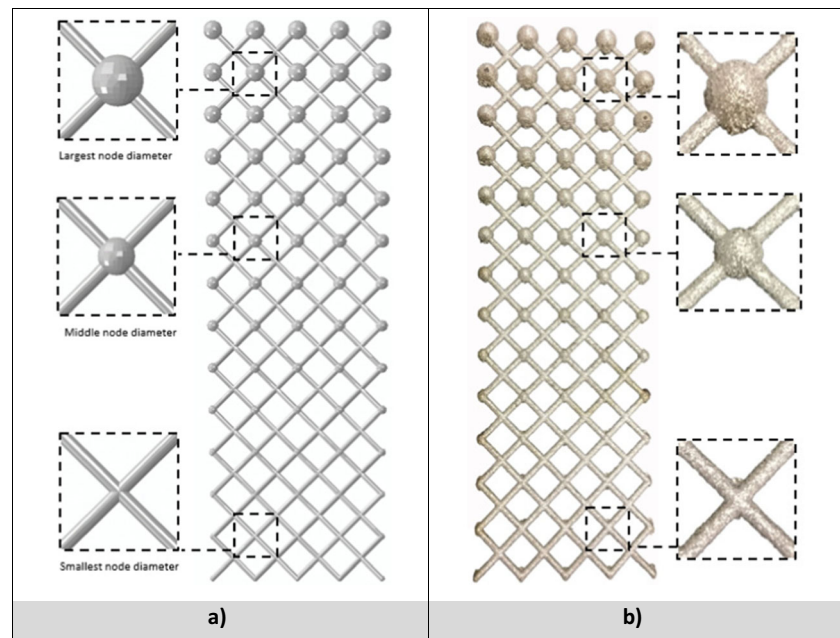
### 4.1 Lattice structure design and manufacture

The proposed method is based on the acquisition of transmitted light images of as-manufactured lattice geometry; these images provide a distinct definition of the lattice boundary,

**Table 1** SLM processing parameters

Parameter	Value
Laser power [J/s]	175
Laser velocity [mm/s]	710
Hatch spacing [ $\mu\text{m}$ ]	120
Layer thickness [ $\mu\text{m}$ ]	30

**Fig. 9** a Idealised CAD and (b) as-manufactured geometry of lattice structure with multiple node sizes within single structure



allowing automated numerical analysis. To demonstrate this method, lattice structures were manufactured in Ti-6Al-4V by SLM. The particle size distribution of the powder used is presented in Fig. 8 and the SLM processing parameters used for lattice manufacture are presented in Table 1.

Lattice structure geometries were generated using the open-source programmable lattice generation (PLG) method [38]. This method requires that the lattice topology and geometry, including strut and node diameters, be defined in a standard manner. This data then allows the automated generation of customisable lattice structures, as are required for this research.

The proposed methodology is based on the analysis of individual unit cells. However, for efficient specimen fabrication, lattice specimens were manufactured with node diameters increasing through the height of the structure, thereby enabling analysis of multiple unique unit cells within the fabricated specimens (Fig. 9). To investigate the effects of cell size and strut and node diameters, a full factorial design of experiments was generated (Table 2). Strut diameter was maintained below 1 mm as this geometry has been shown to largely mitigate the dependence of cooling rate on build height for the FCC topology [39]. Node diameters ( $D_n$ ) were dependent strut diameters ( $D_s$ ) and so are described by their node-to-strut diameter ratio ( $D_n/D_s$ ).

It should be noted that, if the node-to-strut diameter is less than  $\sqrt{2}$  (approximately 1.41), then the node diameter will be smaller than the intersection of the struts, and so functionally, it will be as if no node is present at all. To demonstrate this,

specimens were manufactured with node-to-strut diameter ratios below this value (1 and 1.25) and slightly above (1.5).

## 4.2 Microscope image acquisition and processing

For the identification of manufacturing defects and surface morphology of as-manufactured lattice structures, micrographs and transmitted light microscope images were acquired using a Keyence VHX-5000 microscope. An example of a confocal and transmitted light image of a lattice cell is presented in Fig. 10. Six repetitions of each permutation of cell size, node size, and strut size were collected.

As the diameter of as-manufactured nodes varies significantly, a means of quantifying the size of as-manufactured nodes is necessary. For this reason, the minimum ( $D_{\min}$ ) and maximum ( $D_{\max}$ ) dimensions of as-manufactured nodes were measured in the build direction (BD) and the direction perpendicular to the build direction, referred to as the non-build direction (non-BD).

## 4.3 FE model

Transmitted light images (Fig. 11(a)) are automatically cropped to show only a single cell and analysed to identify the 2D boundary of the struts and nodes (Fig. 11(b)). A 2D continuum FE model is then generated within this boundary using a quad element mesh. The 2D representation of the 3D node requires a choice between a plane stress model (suitable

**Table 2** Design of experiments

Cell sizes (mm)	Strut diameters ( $D_s$ ) (mm)	Node-to-strut diameter ratios ( $D_n/D_s$ )
5, 7	0.4, 0.6, 1.0	1.0, 1.25, 1.5, 1.75, 2.0, 2.25, 2.5, 2.75, 3.0, 3.25, 3.5, 3.75

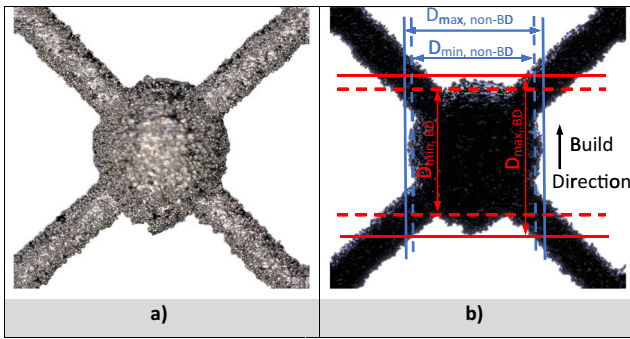


**Fig. 10** **a** Confocal and **(b)** transmitted light microscope images of lattice structure nodes. **b** Minimum ( $D_{min}$ ) and maximum ( $D_{max}$ ) node dimensions in the build direction (BD) and non-build direction (non-BD) are shown

for thin structures) and a plane strain model (suitable for thick structures). The nodes have similar in-plane and out-of-plane dimensions, so the true behaviour of the nodes is expected to lie between the ideal implementation of the plane stress and plane strain techniques. The plane stress model was selected as the more conservative, after applying both options to a sample 2D boundary and determining that the plane stress model yielded at (15%) lower load than the plane strain model.

Boundary conditions are applied to the lateral edges of the cropped image (Fig. 12) as presented in Table 3. A displacement boundary condition is applied to the lower edges, which is iteratively increased until the failure criterion is reached.

A custom material model was generated using tensile specimens fabricated with the SLM parameters and Ti-6Al-4V powder used in the lattice structures and tested according to ASTM Standard E8/E8M-09 [40] (Fig. 13). A virtual model of the tensile specimen was simulated to ensure convergence of the numerical model developed in this research (Section 4.5).

**4.4 Failure criterion**

The maximum Von Mises stress ( $\sigma_{VM}$ ), reaction force at the upper (red) edges ( $F$ ), and displacement of the lower (magenta) edges ( $d$ ) are measured for each numerical iteration

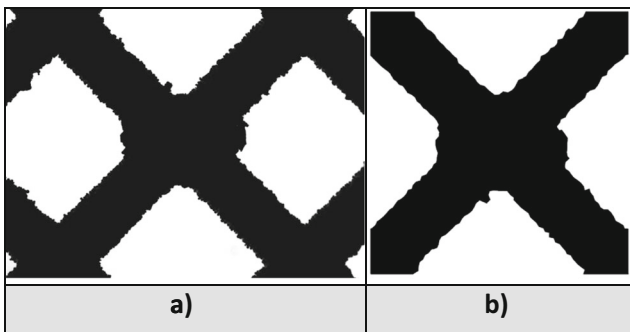


**Fig. 11** **a** Original transmitted light image and **(b)** cropped image generated from boundary extracted from original image by algorithmic image processing

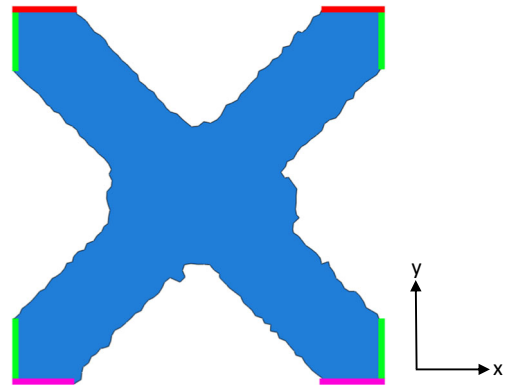


**Fig. 12** Abaqus model generated from extracted boundary including upper (red), lateral (green), and lower (magenta) edges to which boundary conditions are applied

(Fig. 12). Displacement is iterated until the failure criterion is observed, which, in this application, is defined as the development of a plastic hinge within the node element. A plastic hinge is defined as ‘the localised zone of yielding where the moment capacity is reached’ [41]. For the purposes of this model, a plastic hinge is considered to have occurred once plasticity spans across all lattice strut elements (Fig. 14).

The proposed methodology is valid for the failure mode of plastic collapse in the node region; however, it is anticipated that this methodology will be extended to accommodate alternate failure modes, in particular the fatigue failure mode which is of significant relevance to safety-critical applications, for example [42, 43].

To convert the load applied to a lattice structure to a stress value, the conventional method is to divide the load by the initial cross-sectional area of the lattice base [44]. As the model uses plane stress elements, stress is calculated by dividing the reaction force by the product of the width of the unit cell (either 5 or 7 mm) and the plane stress element thickness. The strength of the structure ( $\sigma_f$ ) is defined as the stress when the failure criterion is met.

Stiffness is defined as the ratio of reaction force to displacement at the onset of plastic hinges within all strut elements (Eq. 3).

$$k = \frac{F}{d} \tag{3}$$

where

**Table 3** Numerical model boundary conditions

Edge	Colour	Constrained displacements	Constrained rotations
Upper	Red	$x, y$	$z$
Lateral	Green	$x$	$z$
Lower	Magenta	$x$	$z$

- $k$  Lattice cell stiffness (N/mm)  
 $F$  Reaction force measured at upper edges (N)  
 $d$  Displacement of lower edges (mm)

The variables  $\sigma_{VM}$ ,  $F$  and  $d$  were acquired at each displacement increment up to the onset of plastic hinges, while  $\sigma_f$  represents the stress required to cause adequate deformation for plastic hinges to occur.

#### 4.5 Validation

Finite element mesh convergence was tested by comparing reaction force and associated simulation time for a specified mesh refinement (Table 4). Convergence was determined by a change of reaction force less than 1%. Based on this analysis, a mesh seed size of 0.05 mm was used in custom scripts to allow automated model generation. To ensure the validity of the proposed numerical simulation, a model was generated that combined the generated cell geometry and a virtual representation of the tensile specimen geometry (Section 4.3). The numerical simulation and experimental test data converge, thereby confirming the validity of the numerical simulation (Fig. 15).

### 5 Results and discussion

Results of the analyses provide insight into the difference between the idealised CAD and as-manufactured geometry, the effects of design parameters on strength and stiffness of the manufactured structures, and the comparative performance of models generated from idealised CAD and as-manufactured geometry.

Examples of as-manufactured and idealised CAD cell geometries for 5 mm cell size and different node and strut diameters are presented in Fig. 16.

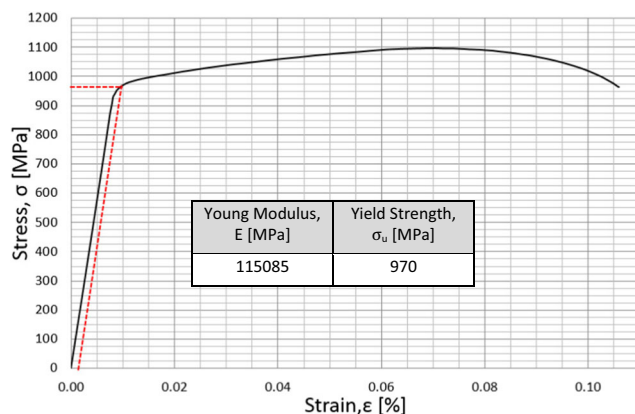


**Fig. 13** Stress-strain response of SLM Ti-6Al-4V tensile test specimens according to ASTM Standard E8/E8M-09

#### 5.1 Comparison between idealised and as-manufactured node sizes

The idealised CAD and as-manufactured node dimensions in both the build and non-build directions are compared for 5 mm and 7 mm cell sizes in Fig. 17 with the following observations:

- Both the minimum and maximum as-manufactured node dimensions are typically larger than for the idealised CAD geometry. Even for the idealised CAD with no node geometry (Fig. 16(a)), material adheres to the upper and lower surfaces at the strut intersection during fabrication. However, for the 1000- $\mu\text{m}$  diameter struts, nodes with diameters larger than 2.5 mm have a minimum node diameter below that of the idealised CAD. In these scenarios, additional particles adhere to upper and lower surfaces, increasing node size in the build direction, but with less observed effect in the non-build direction.
- For specimens with node-to-strut diameter ratios less than or close to  $\sqrt{2}$ , the node diameters were essentially constant, as the diameter of the node does not exceed the dimensions of the intersection of the struts, as previously discussed.
- For most geometry, the idealised CAD diameter was closest to the as-manufactured diameter in the non-build direction; this observation is due to the preferential adhesion of particles to upper and lower node surfaces.
- Fotovvati et al. found geometric errors are increased in layers further from the build platen due to ‘increase in the porosity and prior  $\beta$  grain width with increasing height, which is affected by cooling mechanisms’ [45]. However, error in as-manufactured node size was found to be quite constant with increasing node size, which, due to the design of specimens, was itself a function of height, suggesting this phenomenon was not significant. Rather, the difference between the as-manufactured and idealised CAD node diameters appears to be somewhat constant when node sizes exceed the size of strut intersections

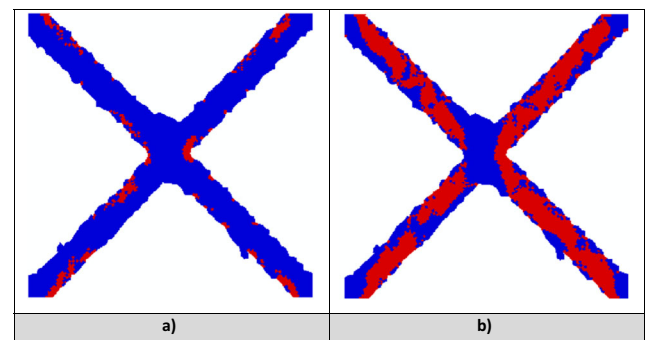


**Fig. 14** Example of analysis results. **a** No plastic hinge (plastic deformation extends only partially through the structure). **b** Plastic hinge identified (plastic deformation extends through structure). Elastic regions are presented in blue, plastic regions in red



**Table 4** Model convergence to predict reaction force with mesh seed sizes 0.07 mm, 0.05 mm, 0.025 mm, and 0.0125 mm

Mesh size [mm]	0.07	0.05	0.025	0.0125
Reaction force [N]	10837	10912	10942	10936.3
Incremental difference in reaction force [%]	-	0.69	0.27	0.05
Simulation time [s]	21	24	71	230

and seems to be related to general geometric errors associated with the SLM process. However, as all node diameters for a given strut diameter were fabricated at the same height, it is difficult to directly assess this effect, suggesting an opportunity for further research.

These initial findings suggest that lattice as-manufactured geometries are generally larger than the idealised CAD, although this occurs preferentially in the build direction. Furthermore, the minimum manufacturable node size is dependent on the lattice structure node size, strut size, and cell size. Further research is required to fully quantify the relationship between idealised CAD and as-manufactured geometry.

**5.2 Effect of node size on maximum stress**

The stress concentrating effects of the as-manufactured node geometry was examined at load displacements lower than required to cause plasticity. The effect of node size on the maximum Von Mises stress within the models at 0.001 mm displacement of the southern edges is presented in Fig. 18 with the following observations:

- Increasing strut element size increases the resistance to deformation and consequently increases the stress required to achieve a specified strain of the unit cell. Increasing node size reduces the available length, thereby leading to a greater stress concentration with increased node size.

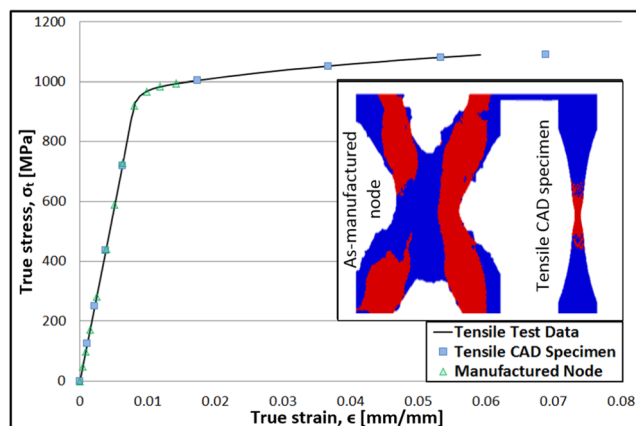


**Fig. 15** Convergence of tensile test data and numerically simulated stress-strain behaviour of tensile CAD specimen and MAM node acquired by the proposed method

- Five-millimetre cells were found to have greater maximum Von Mises stress at 0.001 mm displacement compared with 7-mm cells. As strut and node diameter remain constant but strut element length increases with cell size, struts are relatively shorter in the 5-mm cells. As stated above, this increases the local stress required within individual strut elements to achieve a given lattice strain, leading to larger stress in the shorter strut elements of the 5-mm unit cell.
- As can be seen in Fig. 16 (a) and (b), as-manufactured nodes are larger in the build direction due to the preferential adhesion of particles on upper and lower node surfaces, resulting in as-manufactured node geometry with an approximately elliptical geometry with major axis aligned to the build direction. The mechanical consequence of this node geometry is that a greater stress is observed when models are loaded in the non-build direction, although the magnitude of this effect is relatively slight. However, as identified earlier, this effect may be more pronounced if the failure criteria were fatigue rather than plastic collapse.

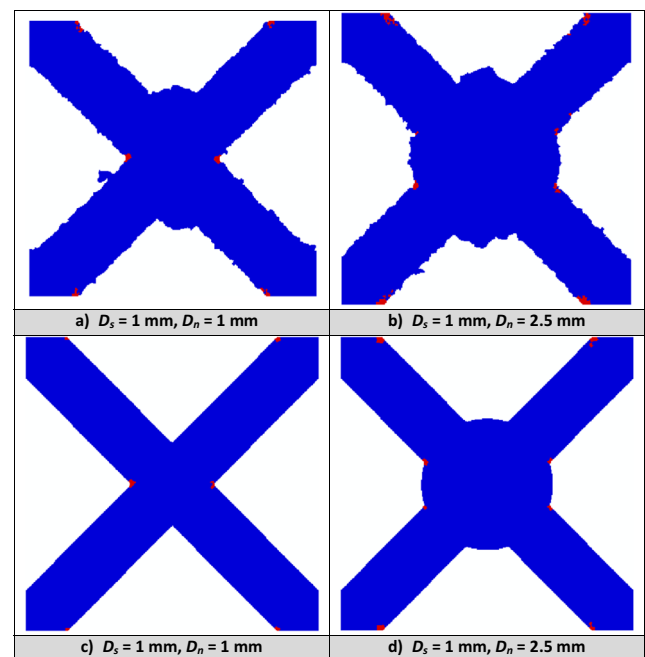


**Fig. 16** Examples of as-manufactured ((a), (b)) and idealised CAD ((c), (d)) geometry for 5 mm cell size at 0.001 mm displacement. Blue regions are elastic; red regions are plastic. All specimens were loaded parallel to the build direction (upward in these images)

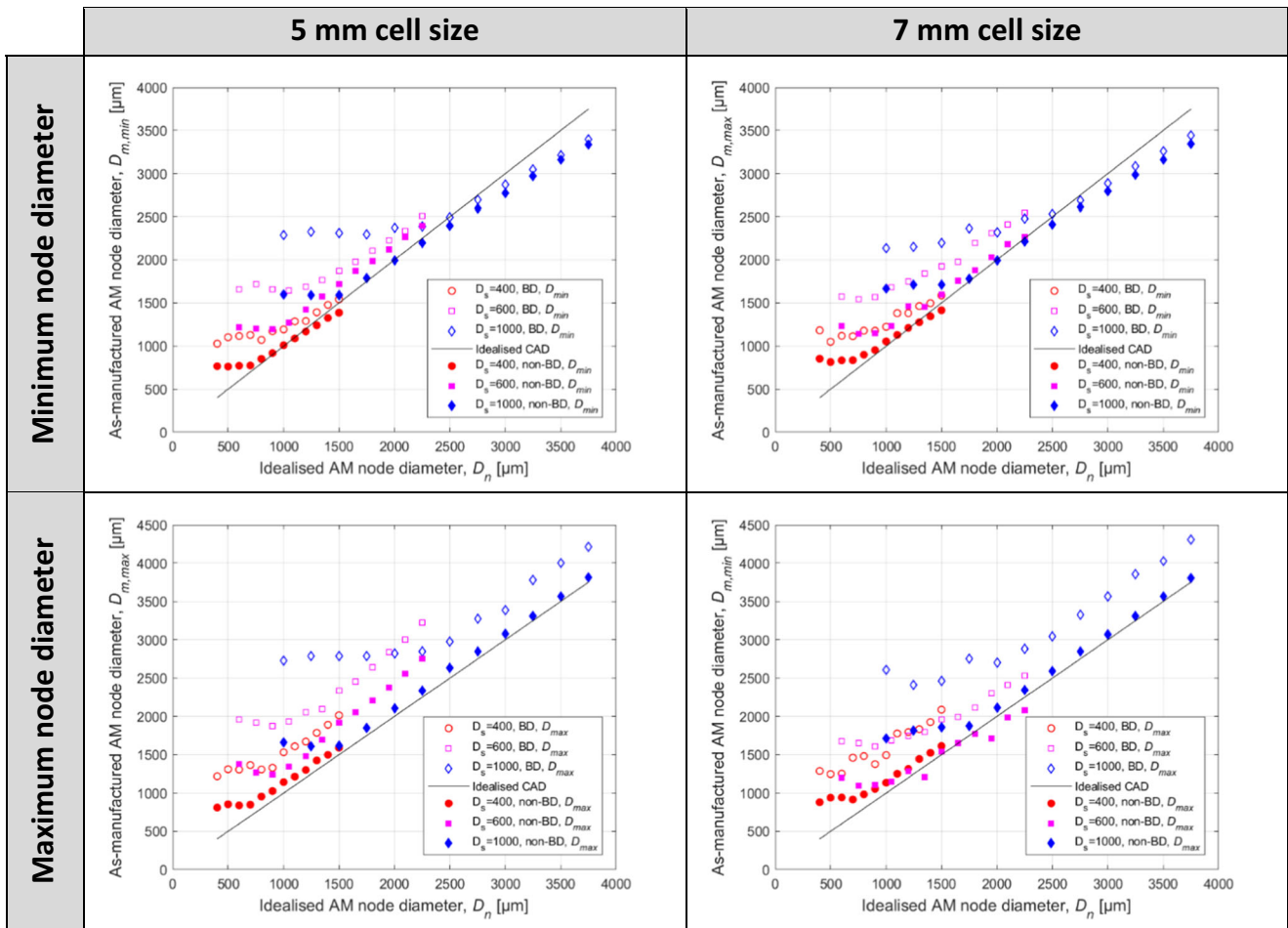


Fig. 17 Comparison of minimum and maximum node diameter for idealised CAD and as-manufactured node diameters for 5- and 7-mm cell sizes

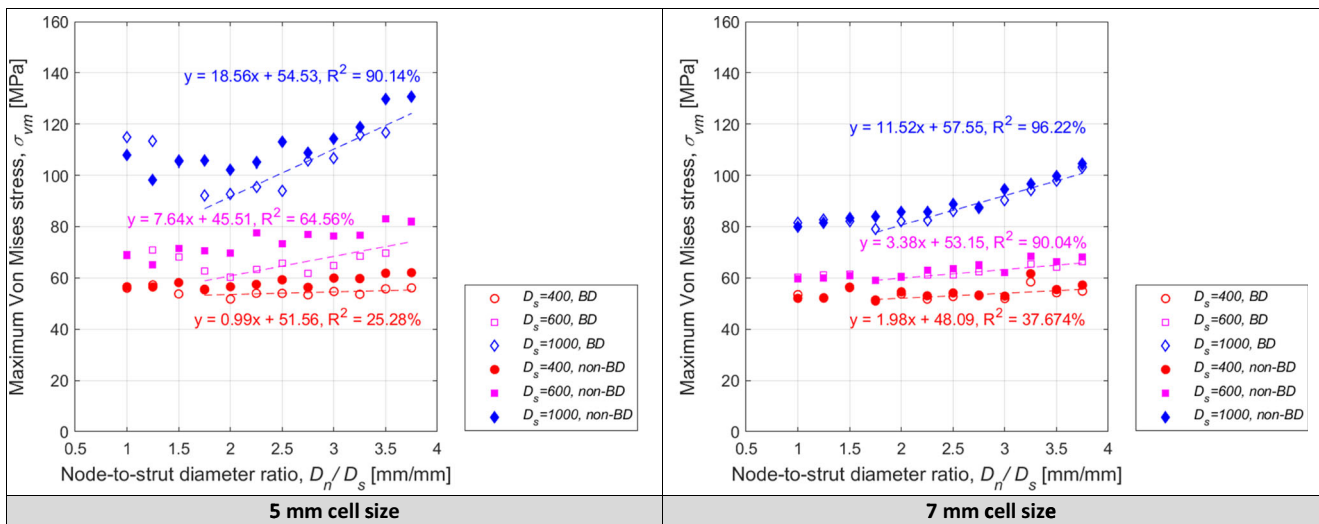


Fig. 18 Maximum Von Mises stress at 0.001 mm displacement for 5-mm and 7-mm cell sizes and varying node-to-strut diameter ratio. Box identifies node-to-strut diameters that result in no node being present in the idealised CAD geometry

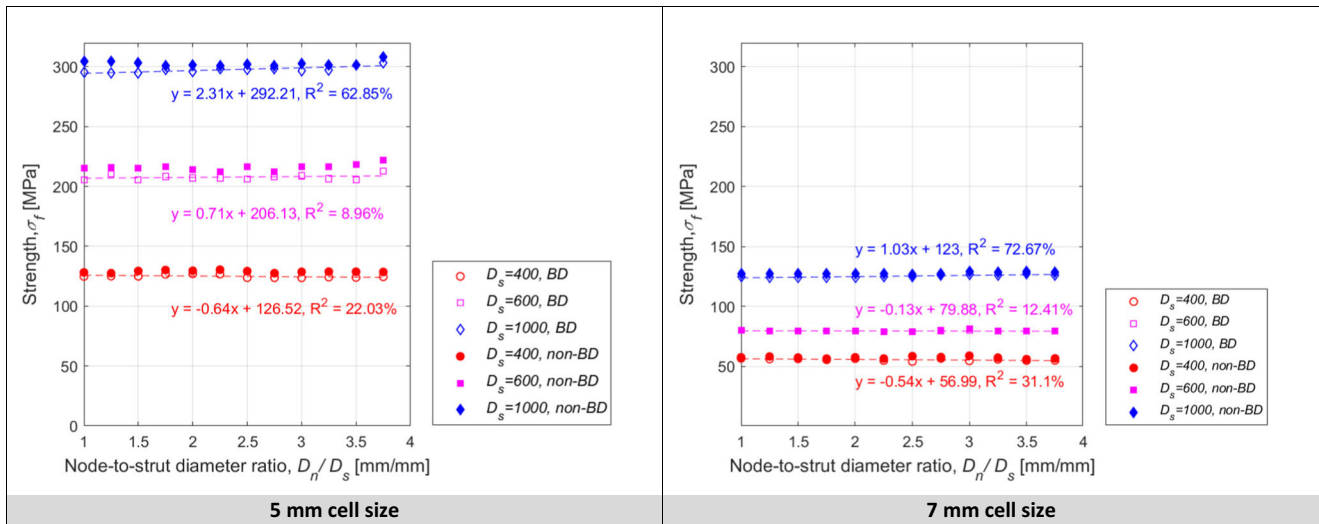


Fig. 19 Strength at observation of plastic hinges for 5-mm and 7-mm cell sizes and varying strut and node diameters

### 5.3 Effect of node diameter on lattice strength and stiffness

Extending the load displacements to the point of failure of the node (the development of plastic hinges through the entire node or across all four struts) determined the node’s strength. The strengths of specimens are compared in Fig. 19 with the following observations:

- The strength of the node structures can be seen to be related to strut diameter and cell size. Strength increases with strut diameter, as would be expected due to the greater load bearing area of these larger sections. Similarly, reduced cell size results in increased relative density and an increased relative

cross-sectional area to support the external loading [10].

- Node diameter has little effect on the observed strength of these lattice structures. As can be seen in Fig. 16, stress concentrations occur at the intersection of strut and node elements; however, the failure mode defined for this research requires a plastic hinge to develop, which is typically observed across the strut elements. Consequently, resistance to failure is highly dependent on strut element diameter.
- Little quantitative difference is observed between strengths in build and non-build directions, although the strength in the non-build direction is marginally higher than is observed in the build direction. For failure modes such as fatigue, this difference may be more pronounced.

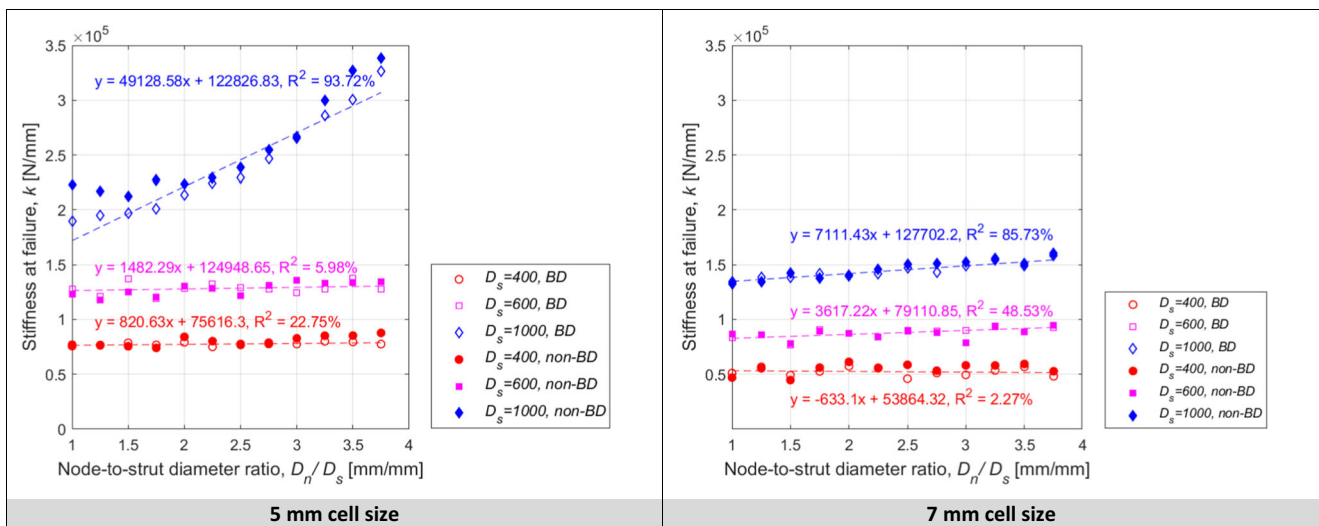


Fig. 20 Lattice structure stiffness for different cell sizes and node and strut diameters

The stiffness for different unit cell scenarios is presented in Fig. 20 with the following observations:

- Stiffness increases with increasing node-to-strut diameter ratio, especially for larger diameter strut elements at the smaller cell size. This observation suggesting increase in stiffness is related to the actual size of the node, not just its ratio to the strut — as the nodes were larger on larger struts, the increase in stiffness was greater.
- The stiffness of 5-mm cells was greater than the stiffness of 7-mm cells for a given strut diameter. Like strength, stiffness is understood to increase with relative density due to more material being present to resist deformation, and as the 5-mm cells had greater relative density, they were stiffer than the 7-mm cells.
- Stiffness was generally greater in the non-build direction. As already discussed, the non-build direction node diameter was consistently greater than the build direction diameter, and as increased node diameter increases stiffness, models were stiffer when loaded in the non-build direction.

### 5.4 Comparative performance of idealised CAD and as-manufactured geometry

The stiffness and strength of as-manufactured and CAD geometries of lattice structures with 5-mm cell size are compared in Fig. 21 with the following observations:

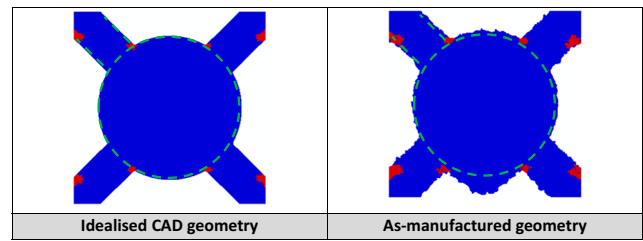


**Fig. 22** Relative node size of idealised CAD and as-manufactured geometry for identical input parameters ( $D_n = 3750 \mu\text{m}$ ,  $D_s = 1000 \mu\text{m}$ , displacement = 0.035 mm). The build direction for the as-manufactured geometry is upward

- As-manufactured geometry is consistently stronger and stiffer than for CAD geometry. This observation occurs as as-manufactured geometry is typically associated with larger strut and node element sizes than for the idealised CAD, which strengthens and stiffens the as-manufactured structures (Fig. 22).
- The simulation of the idealised CAD geometry underestimates the response of the as-manufactured geometry by a consistent amount. This outcome suggests that numerical analysis of the idealised CAD can be used as a proxy to provide estimates of the actual strength and stiffness of as-manufactured geometries.
- As with strength and stiffness, there is an observed inconsistency for  $D_n/D_s \leq 1.75$ . For these specimens, the node diameter is smaller than the strut intersection, meaning that there effectively was no node geometry, as previously discussed.
- Regression analysis was performed to relate the strength and stiffness of CAD and as-manufactured geometries, resulting in Eqs. 4 and 5, each of which showed high

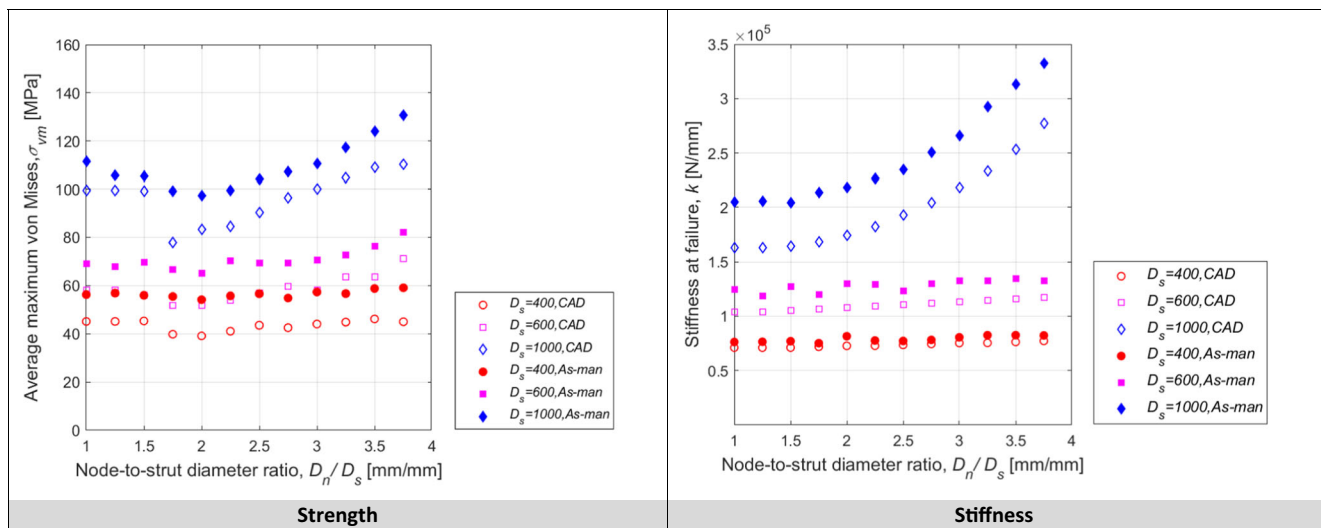


**Fig. 21** Comparison between as-manufactured and CAD response. Maximum von Mises stress at 0.001 mm for 7-mm cell size and stiffness at failure for 5-mm cell sizes

correlation, with  $R^2 = 99\%$  and  $98\%$ , respectively. These formulae allow designers to predict the behaviour of as-manufactured geometries based on the performance of CAD geometries with very high confidence, negating

the need for microscope images of as-manufactured geometries.

$$k_{AM} = -146,174 + 14,019 \frac{D_n}{D_s} + 18,089 l_c + 3.4791 k_{CAD} - 0.000001 k_{CAD}^2 - 1,734 \frac{D_n}{D_s} l_c - 0.0565 \frac{D_n}{D_s} k_{CAD} - 0.3276 l_c k_{CAD} \quad (4)$$

$$\sigma_{AM} = -15.33 + 2.2 \frac{D_n}{D_s} + 6.229 l_c + 1.731 \sigma_{CAD} + 1.193 \frac{D_n^2}{D_s} + 0.0636 \frac{D_n}{D_s} \sigma_{CAD} - 0.1788 l_c \sigma_{CAD} \quad (5)$$

where

$k_{AM}$	Stiffness of the as-manufactured geometry (N/mm)
$k_{CAD}$	Stiffness of the ideal CAD geometry (N/mm)
$\sigma_{AM}$	Strength of the as-manufactured geometry (MPa)
$\sigma_{CAD}$	Strength of the ideal CAD geometry (MPa)
$\frac{D_n}{D_s}$	Ratio of node diameter ( $D_n$ ) to strut diameter ( $D_s$ )
$l_c$	Cell size (mm)

## 6 Conclusion

In this paper, a novel method for evaluating the effects of cell size and node and strut diameters on the performance of Ti-6Al-4V SLM lattice structures has been proposed. The method involves automated FE analysis of 2D models generated from transmitted light microscope images of as-manufactured lattice geometries. Insights provided by the results of this analysis include:

- As-manufactured geometries are generally larger than input CAD geometries due to geometric defects inherent in the manufacturing process. Consequently, the as-manufactured geometry outperforms the idealised CAD in terms of strength and stiffness due to the greater amount of material present to resist deflection.
- The strength of a lattice structure is dependent on cell size and strut diameter, with little observed effect of node diameter. Observed failure occurs at the intersection of strut elements with the node; this plastic failure event is largely independent of the associated node diameter. Note that this outcome may be contrary to observations for fatigue response, where stress concentration magnitude (rather

than plastic hinge formation) is the primary failure predictor.

- Increasing the size of nodes and strut elements increases the stiffness of structures, again due to the presence of additional strengthening material. However, decreasing cell size also improves strength and stiffness due to the resultant increase in the relative density of the structure.
- Maximum nodal diameters were generally found to be larger perpendicular to the build direction due to manufacturability limitations. The result of this is that as-manufactured geometries generally performed better when loaded perpendicular to the build direction, due to a greater presence of material. This outcome has a more significant influence on the strength of the structure rather than its stiffness.
- Comparison between the performance of idealised CAD and as-manufactured geometry indicates that the idealised CAD models always underpredicts the strength and stiffness of the structure. However, the extent of this underprediction was consistent. A regression analysis was used to relate CAD and as-manufactured results with very high correlation ( $\sim 99\%$ ). This identified relationship means that, for future analyses, manufacture of specimens is unnecessary, and idealised CAD results can be corrected to provide a robust prediction of the performance of as-manufactured lattice structures.
- These findings are based on 2D models developed from the silhouette of lattice nodes, and further research is expected to extend these concepts, for example application to 3D lattice structures; accommodation of residual stress effects; and the extension of this methodology to accommodate alternate failure modes including fatigue. It is hoped that the methodology proposed in this research will provide a valuable basis for the further understanding of the effect of process parameters, topology, and geometry on the mechanical efficiency of as-manufactured lattice structures.

**Acknowledgements** This research was conducted by the Australian Research Council Industrial Transformation Training Centre in Additive Biomufacturing (IC160100026). The authors acknowledge the facilities and the scientific and technical assistance of the RMIT Advanced Manufacturing Precinct.

**Funding information** This work was financially supported by the members of the ARC Training Centre for Lightweight Automotive Structures and from the Australian Research Council (Grant Reference IC160100032).

## References

- Zhang XZ et al (2018) Selective electron beam manufactured Ti-6Al-4V lattice structures for orthopedic implant applications: current status and outstanding challenges. *Curr Opin Solid State Mater Sci* 22(3):75–99
- Maconachie T et al (2019) SLM lattice structures: properties, performance, applications and challenges. *Mater Des* 183:108137
- Tao W and Leu MC. (2016) Design of lattice structure for additive manufacturing. In *International Symposium on Flexible Automation (ISFA)*. 2016.
- Zadpoor AA (2018) Mechanical performance of additively manufactured meta-biomaterials. *Acta Biomater*
- Gong H, et al. The effects of processing parameters on defect regularity in Ti-6Al-4V parts fabricated by selective laser melting and electron beam melting. In 24th annual international solid freeform fabrication symposium - an additive manufacturing conference. Austin, Texas.
- Sarker A et al (2018) Angle defines attachment: switching the biological response to titanium interfaces by modifying the inclination angle during selective laser melting. *Mater Des* 154:326–339
- Fotovvati B, Asadi E (2019) Size effects on geometrical accuracy for additive manufacturing of Ti-6Al-4V ELI parts. *Int J Adv Manuf Technol* 104(5):2951–2959
- Dallago M et al (2018) Effect of the geometrical defectiveness on the mechanical properties of SLM biomedical Ti6Al4V lattices. *Proc Struct Integr* 13:161–167
- Van Bael S et al (2011) Micro-CT-based improvement of geometrical and mechanical controllability of selective laser melted Ti6Al4V porous structures. *Mater Sci Eng A* 528(24):7423–7431
- Gibson LJ and Ashby MF, (1999) *Cellular solids: structure and properties*. Cambridge university press.
- Xiao Z et al (2018) Evaluation of topology-optimized lattice structures manufactured via selective laser melting. *Mater Des* 143:27–37
- Banhart J (2000) Manufacturing routes for metallic foams. *Jom* 52(12):22–27
- He M, Hu W (2008) A study on composite honeycomb sandwich panel structure. *Mater Des* 29(3):709–713
- Yan C et al (2014) Evaluation of light-weight AlSi10Mg periodic cellular lattice structures fabricated via direct metal laser sintering. *J Mater Process Technol* 214(4):856–864
- Leary M et al (2016) Selective laser melting (SLM) of AlSi12Mg lattice structures. *Mater Des* 98:344–357
- Yan C et al (2014) Advanced lightweight 316L stainless steel cellular lattice structures fabricated via selective laser melting. *Mater Des* 55:533–541
- Vandenbroucke B, Kruth J-P (2007) Selective laser melting of bio-compatible metals for rapid manufacturing of medical parts. *Rapid Prototyp J* 13(4):196–203
- Leary M et al (2019) Mechanical and thermal characterisation of AlSi10Mg SLM block support structures. *Mater Des* 183:108138
- Wauthle R et al (2015) Effects of build orientation and heat treatment on the microstructure and mechanical properties of selective laser melted Ti6Al4V lattice structures. *Addit Manuf* 5:77–84
- Yavari SA et al (2015) Relationship between unit cell type and porosity and the fatigue behavior of selective laser melted meta-biomaterials. *J Mech Behav Biomed Mater* 43:91–100
- Santorinaios M, et al., (2006) Crush behaviour of open cellular lattice structures manufactured using selective laser melting. *WIT Trans Built Environ* 85.
- Yan C et al (2012) Evaluations of cellular lattice structures manufactured using selective laser melting. *Int J Mach Tools Manuf* 62:32–38
- Fox JC, Moylan SP, Lane BM (2016) Effect of process parameters on the surface roughness of overhanging structures in laser powder bed fusion additive manufacturing. *Procedia CIRP* 45:131–134
- Leary M (2017) 4 - Surface roughness optimisation for selective laser melting (SLM): accommodating relevant and irrelevant surfaces, in *Laser Additive Manufacturing*, M. Brandt, Editor, Woodhead Publishing, p. 99-118.
- Mullen L et al (2010) Selective laser melting: a unit cell approach for the manufacture of porous, titanium, bone in-growth constructs, suitable for orthopedic applications. II. Randomized structures. *J Biomed Mater Res B Appl Biomater* 92B(1):178–188
- Islam M et al (2013) Temperature profile and imaging analysis of laser additive manufacturing of stainless steel. *Phys Procedia* 41: 835–842
- Kurzynowski T, et al. (2012) Parameters in selective laser melting for processing metallic powders. In *Proceedings of SPIE - The International Society for Optical Engineering*
- Bächle M, Kohal RJ (2004) A systematic review of the influence of different titanium surfaces on proliferation, differentiation and protein synthesis of osteoblast-like MG63 cells. Eine systematische Uebersicht über den Einfluss von verschiedenen Titanoberflächen auf die Proliferation, Differenzierung und Proteinsynthese von osteoblastenähnlichen MG63 Zellen. *Clin Oral Implants Res* 15(6):683–692
- Deligianni DD et al (2000) Effect of surface roughness of hydroxyapatite on human bone marrow cell adhesion, proliferation, differentiation and detachment strength. *Biomaterials* 22(1):87–96
- Lincks J et al (1998) Response of MG63 osteoblast-like cells to titanium and titanium alloy is dependent on surface roughness and composition. *Biomaterials* 19(23):2219–2232
- Wennerberg A, Albrektsson T (2009) Effects of titanium surface topography on bone integration: a systematic review. *Clin Oral Implants Res* 20:172–184
- Kim HJ et al (2005) Varying Ti-6Al-4V surface roughness induces different early morphologic and molecular responses in MG63 osteoblast-like cells. *J Biomed Mater Res A* 74A(3):366–373
- Bowers KT et al (1992) Optimization of surface micromorphology for enhanced osteoblast responses in vitro. *Int J Oral Maxillofac Implants* 7(3):302–310
- Jemat A et al (2015) Surface modifications and their effects on titanium dental implants. *Biomed Res Int* 2015:791725
- Frazier WE (2014) Metal additive manufacturing: a review. *J Mater Eng Perform* 23(6):1917–1928
- Liu Y, Yang Y, Wang D (2016) A study on the residual stress during selective laser melting (SLM) of metallic powder. *Int J Adv Manuf Technol* 87(1):647–656
- Ali H et al (2017) In-situ residual stress reduction, martensitic decomposition and mechanical properties enhancement through high temperature powder bed pre-heating of Selective Laser Melted Ti6Al4V. *Mater Sci Eng A* 695:211–220
- McMillan M et al (2015) Programmatic lattice generation for additive manufacture. *Procedia Technology* 20:178–184

39. Downing D et al (2020) Heat transfer in lattice structures during metal additive manufacturing: numerical exploration of temperature field evolution. *Rapid Prototyp J*
40. Xu W et al (2017) In situ tailoring microstructure in additively manufactured Ti-6Al-4V for superior mechanical performance. *Acta Mater* 125:390–400
41. Gorenc B, et al. (2005) *Steel designers' handbook*. UNSW Press.
42. Feng Q et al (2016) An investigation into the quasi-static response of Ti6Al4V lattice structures manufactured using selective laser melting, in *Smart Innovation. Systems and Technologies* 52:399–409
43. Fotovvati B, Namdari N, Dehghanghadikolaei A (2018) Fatigue performance of selective laser melted Ti6Al4V components: state of the art. *Materials research express* 6(1):012002
44. Mazur M et al (2016) Deformation and failure behaviour of Ti-6Al-4V lattice structures manufactured by selective laser melting (SLM). *Int J Adv Manuf Technol* 84(5):1391–1411
45. Fotovvati B, Etesami SA, Asadi E (2019) Process-property-geometry correlations for additively-manufactured Ti-6Al-4V sheets. *Mater Sci Eng A* 760:431–447

**Publisher's note** Springer Nature remains neutral with regard to jurisdictional claims in published maps and institutional affiliations.